Soft-x-ray-induced secondary-electron emission from semiconductors and insulators: Models and measurements

Burton L. Henke, John Liesegang,* and Steven D. Smith
University of Hawaii, Department of Physics and Astronomy, Honolulu, Hawaii 96822
(Received 27 July 1978)

Secondary-electron energy distribution curves (EDC's) and the total secondary-electron yields relative to such for gold have been measured for seven semiconductors for which electron-electron scattering losses within the emitter were considered dominant and for nine insulators (alkali halides) for which electron-phonon scattering losses were expected to be dominant in the transport process. The secondary-electron spectra were excited by Al-$K\alpha$ (1487 eV) photons and were measured from evaporated dielectric films (of about 0.3 μ thickness) on conducting substrates with an electrostatic hemispherical analyzer of about 0.03-eV resolution. Some of the dielectric photoemitters have appreciably narrower energy distributions and higher yields than has gold; CuI and CsI have EDC widths at half-maximum of about one-third of that for gold, and yield values of 11 and 30 times greater. The FWHM and secondary-electron yield for gold were measured to be about 4 eV and 0.50 electrons per normally incident photon, respectively. The shapes of the EDC's were found to be essentially unchanged for photon excitation in the 0.1–10-keV region. Strong structural features appear only in the alkali halide EDC's, and it is proposed that these are mainly the result of single-electron promotion of secondaries from the valence band by plasmon deexcitation. A relatively simple model for x-ray photoemission has been developed which assumes that direct excitation of secondaries by photoelectron and Auger-electron "primaries" is the dominant excitation mechanism, and accounts for both electron-electron and electron-phonon scattering in the transport process. Free-electron conduction-band descriptions are assumed. The theoretical and experimental curves are in satisfactory agreement.

I. INTRODUCTION

There has been a considerable amount of effort on the theory and application of secondary-electron emissions using electron excitation in the kilovolt region (as applied, for example, in scanning microscopy) and using extreme ultraviolet excitation (as applied in band-structure analysis). There has been relatively little theoretical or experimental work reported on the generation of the secondary electrons using x-ray excitation (which is of considerable current interest as applied to the measurement of the intensity and the temporal history into the picosecond region of pulsed x-ray sources with the diode detector, the streak, and the framing cameras in high-temperature plasma diagnostics).

With electron and extreme ultraviolet generation of the secondary-electron distribution, the effective escape depths of the electrons can be very dependent upon the attenuation mechanism of the exciting radiation. With x-ray excitation of the photoelectron and subsequent emission of the associated Auger-electron "primaries" which in turn generate the internal secondary-electron distribution, the electron escape depths are usually independent of the x-ray attenuation process. This is because the x-ray penetration is very large as compared to the effective electron escape length. Thus with x-ray excitation, often a more direct and precise interpretation of the secondary-electron energy distribution can be made in terms of models for the excitation, transport, and escape processes.

In an earlier work,[1] the electron energy dependence of the secondary-electron energy distribution from metals as excited by x-rays in the 0.1–10-keV region was measured and found to be consistent and predictable by applying currently available theoretical descriptions for the excitation, mean free paths, and escape for secondaries in metals. In this present work, we have measured the energy dependence and relative yields of the secondary electrons as excited by soft x rays (principally at 1487-eV photon energy) for a representative series of semiconductors and insulators. For these systems, the secondary-electron generation processes are more complex, particularly for the insulators for which multiple scattering has an appreciable role in the transport process. In order to test available theoretical expressions for the secondary-electron excitation and for the mean free paths for pair production and for electron-phonon interactions for the energy region below 10 eV, we have used the relatively simple rate equation developed by Kane[2] for a description of the multiple scattering transport process. We believe this approach will be helpful at this time in guiding the application of more exact transport theories, analytical and numerical, in later studies.

In Sec. II, we present the "semiclassical," simple case for x-ray excited secondary- electron generation for the "no-loss" transport (no multi-

ple inelastic scattering) which is the limiting case for the semiconductors when only strong electron pair production need be considered. We are thus able to define specifically in this context our model for the roles of the x-ray generation and the escape of secondary electrons which are applicable to all materials—metals, semiconductors, and insulators. We then apply the Kane rate equation to include the additional effects of multiple scattering and we also introduce a simple accounting for the accumulated electron-phonon energy losses.

In Sec. III, we review briefly our methods for measuring the secondary-electron energy distributions, and present such data along with the theoretical curves as based upon our derived models for a selected series of semiconductors and insulators (alkali halides).

In Sec. IV, we discuss the possible origins of the very interesting and often very strong structural features that appear in the secondary-electron energy distributions for the insulators.

II. MODEL FOR THE X-RAY EXCITATION OF SECONDARY-ELECTRON EMISSION

A. Excitation

An x-ray photon is absorbed by an atom within the emitter resulting in the ejection of a photoelectron. The immediate relaxation of the atom is by the emission of a shower of Auger electrons of similar kinetic energies as that of the photoelectron, and by fluorescent photon emission. A small additional number of such electrons are generated by the absorption of some of these secondary radiation photons. Some of these electrons may escape from the emitter surface with little or no loss and as elastically emitted photoelectrons and Auger electrons. The remaining electrons form a class of "primaries" that give up their energy to the generation of low-energy secondary electrons by principally weak interactions through the fast portion of their paths and by more direct collisional interactions through the slower ends of their paths, or alternatively, by the generation of plasmons which, in turn, may deexcite to form low-energy secondaries. These interactions involve almost entirely the promotion of bound-state valence electrons into the conduction band.

We define here, by $X(E)$, the number of secondary electrons thus generated per unit energy interval in E, per unit solid angle, per unit emitter volume, and per unit incident photon intensity. E is the electron energy taken here *as measured from the bottom of the conduction band.* See Fig. 1. Because of the randomizing nature of the processes of secondary-electron generation, the internal electron distribution is assumed to be isotropic.

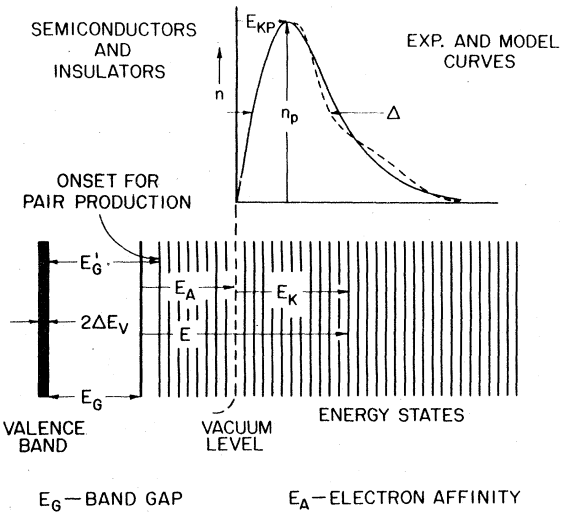

FIG. 1. Simplified energy-level diagram for the dielectric photocathode relating the observed emitted electron kinetic energy E_K to its energy as measured from the bottom of the conduction band, E, and to E_G and E_A, the band-gap and electron affinity energy values. We define here as semiconductors and insulators those materials for which the emitted secondary electrons have energies E greater or less than E'_G, respectively, where E'_G is the energy required for onset of pair production. Assumed for the x-ray photoemission model developed here is an "averaging," free-electron density of states for the conduction band.

$X(E)$ may be related to the single primary-electron excitation functions $S(E)$ in the following way: Let $S(E)$ be the number of secondaries generated per unit interval of their energy E, and per unit path length of the exciting primary electron when its energy is equal to E_p. We make the important assumption that $S(E)$ may be written

$$S(E)=P(E_p)q(E)=P(E_p)[q_f(E)+q_s(E)+q_p(E)]. \quad (1)$$

$q_f(E)$, $q_s(E)$, and $q_p(E)$ give the E-dependent contributions for the fast electron, slow electron, and plasmon deexcitation processes. This assumption will require that the observed E dependence of the emitted secondary distribution is independent of the photon energy E_0, and therefore separable from the "primary-electron" energy dependence. This has been borne out by our experimental measurements for photon energies in the range 0.1–10 keV. [Also, typical theoretical expressions do yield a $p(E_p)$ and one usually of a E_p^{-1} dependence, for direct primary and plasmon deexcitation generation of secondaries in metals, semiconductors, and insulators. See Eqs. (22) and (23).]

We assume that all of the primary-electron energy that is absorbed within the sample is passed on to the generation of an initial internal secondary-

electron distribution $S(E)$, as described above, and therefore the rate of energy loss of a primary electron may be written for semiconductors and insulators as

$$-\frac{dE_p}{dx}=P(E_p)\int_0^{E'}(E+E_G+\Delta E_V)q(E)\,dE\,. \qquad (2)$$

Here E' defines an effective energy limit of the initial internal secondary-electron distribution. ΔE_V is a "half-width" of the valence band and $E_G+\Delta E_V$ is that part of an interaction energy that is required to bring a valence electron to the bottom of the conduction band. Using Eq. (2), we may now integrate $S(E)$ over the entire effective path of a primary electron. The contribution of each primary electron having initial energy E_{p0} to the generation of the internal secondary-electron distribution becomes

$$\left\{\int_{E_{p0}}^{0}\frac{P(E_p)\,dE_p}{(dE_p/dx)}\right\}q(E)=E_{p0}[4\pi\beta q(E)]\,,$$

where we have defined the normalizing constant β by

$$4\pi\beta q=\left[\int_0^{E'}(E+E_G+\Delta E_V)q(E)\,dE\right]^{-1}, \qquad (3)$$

yielding the dimensions of the distribution function $\beta\,q(E)$ to be simply energy squared. This constant, β, must be finite and a function only of the "internal" constants of the material such as E_G (but not of the surface parameter E_A). B can be obtained from theoretical or experimental expressions for the energy-loss rate for primary electrons, dE_p/dx. It cannot be obtained completely from a secondary-electron emission determination of $q(E)$ because such results can only be descriptive of the high-energy tail of the internal distribution function $q(E)$ (i.e., for electron energies greater than the escape energy E_A for the emitted electrons). Finally, if we sum over all of the effective primaries (photoelectrons and Auger electrons) generated per unit volume and per unit photon intensity, we obtain the internal distribution function $X(E)$ as

$$X(E)=\frac{1}{4\pi}\sum_i[E_{p0_i}4\pi\beta q(E)]$$
$$=U_p(E_0)\beta q(E)\,, \qquad (4)$$

where $U_p(E_0)(=\sum E_{p0_i})$ is the total "primary"-electron energy deposited through photon absorption per unit volume and per unit photon intensity that is effective in secondary-electron generation. This quantity, U_p, may be given by

$$U_p(E_0)=\rho E_0\mu(E_0)(1-\phi_f-\phi_p)\exp(-\mu\rho x/\sin\phi)$$
$$=\rho E_0\mu(E_0)f(E_0)\exp(-\mu\rho x/\sin\phi)\,, \qquad (5)$$

where ρ is the mass density and $\mu(E_0)$ is the mass photoionization cross section at photon energy E_0 for the emitter. ϕ_f and ϕ_p are the effective fractions of the absorbed photon energy that are lost to escaping fluorescent and primary-electron radiations, respectively. The fluorescent and primary-electron radiations that escape "downward" into the sample and away from the secondary-emission escape volume near the surface are balanced by similar radiations passing "upward." Essentially, ϕ_f and ϕ_p are the unbalanced fractional losses through the emitter surface. We define the function $f(E_0)$ as a *conversion efficiency factor* for photon excited secondary-electron generation which should decrease slowly with E_0 and with small abrupt drops at absorption edge energies. These absorption edge "drops" should tend to reduce the overall absorption edge effect upon the secondary-electron production (see Fig. 17 of Ref. 1).

The exponential factor introduced in x dependence for $X(E)$ and is different from unity only when the effective escape depth for the secondary electrons is not small as compared with the x-ray attenuation depth $(\mu\rho)^{-1}\sin\phi$ (see Fig. 2).

B. Transport and escape

The transport to a differential surface area dA of the internal secondary electrons from a position (r,θ') within the emitter must be considered for three important cases involving metals, semiconductors, and insulators. In *metals*, the electrons that can escape can also promote electrons from the Fermi sea and thus possibly produce electron pairs of sufficient energy to escape (cascading). This case has been discussed in Ref. 1. In *semi-*

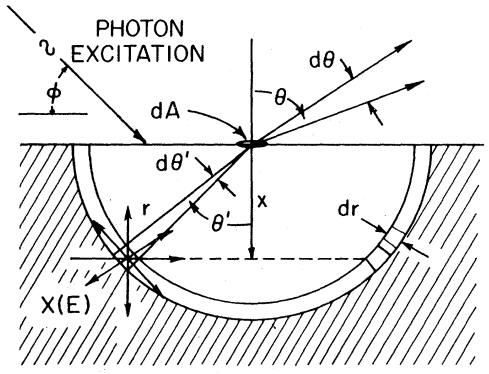

FIG. 2. "No-loss" transport and escape geometry for which those electrons that escape from (r,θ') are assumed to have a survival probability of $\exp(-r/\lambda_e)$, where λ_e is the MFP for pair production. Illustrated here is the refraction of the escaping electron and the associated increase in the differential solid angle of the emitted beam around angle θ.

conductors for which the minimum escape energy E_A is larger than the gap energy E_G, the secondary electrons that can escape can also promote valence electrons into the conduction band. For many semiconductors, however, such scattering leaves the energy of each electron of the pair below the vacuum level, and these electrons cannot escape. Hence, for this case, only those secondaries that survive transport to the surface without such inelastic scattering (the "no-loss" electrons) need be considered for photoemission. In many *insulators* for which those electrons that do escape and constitute the observed secondary-emission spectrum have energies E that are less than the gap energy E_G, this electron-electron scattering is not significant. Then multiple electron-phonon scattering and the associated accumulated energy loss must be considered in describing the transport process. These cases of "no-loss" and of "multiple loss" scattering transport processes for the semiconductors and insulators will now be discussed.

1. "No-loss" electron emission

The number of electrons that survive transport to the surface per unit surface area and per unit photon intensity from the (r, θ') position (see Fig. 2) can be written

$$\frac{dN}{dA\,dE} = X(E)(2\pi \sin\theta' \cos\theta'\, d\theta') \exp\left(-\frac{r}{\lambda_e}\right) dr\,, \quad (6)$$

where we have assumed that the survival fraction can be given by $\exp(-r/\lambda_e)$, λ_e being the mean free path (MFP) for electron-electron scattering that promotes valence electrons into the conduction band. (The differential sample volume involved, as depicted in Fig. 2, is ring-shaped and equal to

$$2\pi r^2 \sin\theta'\, d\theta'\, dr\,,$$

and the solid angle subtended at a point within this volume by the differential area element dA is $dA \cos\theta'/r^2$.)

Assuming λ_e to be small as compared with the x-ray photon attenuation lengths [$X(E)$ independent of position r], we may integrate Eq. (7) from $0 \to \infty$ for the electrons approaching dA in the θ' direction to obtain

$$\frac{dN}{dA\,dE} = X(E)(2\pi \sin\theta' \cos\theta'\, d\theta')\lambda_e\,. \quad (7)$$

Electrons that approach the surface with sufficiently small angles in θ' and with energies greater than the electron affinity energy E_A will refract into the external vacuum region, as illustrated in Fig. 2. Electrons of energy E are slowed down by an electric field which is (on average) normal to the surface and will have an external kinetic energy E_K equal to $E - E_A$. The electrons exit at a larger angle θ and with a larger corresponding total differential solid angle, thus reducing the number of electrons per unit solid angle in the differential emitted beam. To obtain this reduction factor, we assume that the transverse field at the surface is equal to zero and that the transverse momenta of the escaping electrons are thus conserved. Therefore,

$$\sqrt{E}\sin\theta' = \sqrt{E - E_A}\sin\theta\,, \quad (8)$$

yielding the relationship between the angles θ' and θ. Only those electrons of angles θ' less than the critical angle θ_c' for total internal reflection will refract out of the emitter surface. This "escape cone" angle is obtained from Eq. (8) by setting θ equal to 90°, giving the value of θ_c' equal to

$$\sin^{-1}[(E - E_A)/E]^{1/2}\,.$$

The secondary electrons that internally reflect back into the emitter are eventually inelastically scattered into energies below that of the vacuum level and cannot contribute to secondary-electron emission. Squaring and differentiating Eq. (8), we obtain the relation

$$\sin\theta' \cos\theta'\, d\theta' = [(E - E_A)/E] \sin\theta \cos\theta\, d\theta\,,$$

which may be substituted into Eq. (7) to obtain the number of externally refracted electrons in direction θ per unit solid angle, per unit emitter surface area, and per unit photon intensity:

$$\frac{dN}{dA\,dE\,d\Omega} = X(E)\lambda_e\left(\frac{E - E_A}{E}\right)\cos\theta\,. \quad (9)$$

Here we have let $2\pi \sin\theta\, d\theta$ be equated to the external solid angle of emission $d\Omega$.

We define now β, the differential electron optical brightness of the emitter surface per unit energy E and per unit photon intensity, by the relation

$$\frac{dN}{dA\,dE\,d\Omega} = \beta \cos\theta\,. \quad (10)$$

And thus for the "no-loss" secondary-electron emission from a semiconductor, we obtain, from Eqs. (9) and (5),

$$\beta = X(E)\lambda_e[(E - E_A)/E]\,,$$

or

$$\beta = E_0\mu(E_0)f(E_0)\rho\lambda_e Bq(E)[(E - E_A)/E]\,, \quad (11)$$

where, in Eq. (5), we have dropped the x-ray attenuation factor because the x-ray penetration depths $\sim[\mu\rho]^{-1}\sin\phi$ are assumed to be very large as compared with the secondary-electron escape depth $\sim\lambda_e$. [The dependence in Eq. (10) of the secondary-electron emission upon $\cos\theta$ (often described as Lambert's Law follows directly from

our assumption that the internal distribution $X(E)$ is isotropic.]

2. *General "multiple-loss" model for x-ray excited secondary emission*

In the simple "no-loss" model described above, it was assumed that all inelastic scattering in the transport process drops the involved electrons below the vacuum level and that any elastic scattering out of the r direction is compensated by an equally probable elastic scattering into this r direction. We will now attempt to account for the possibility of quasielastic scattering that may involve energy losses that do not immediately drop the involved secondary electrons below the vacuum level (e.g., "multiple-loss" process such as electron-phonon scattering which is of particular interest here). In emitters for which only such small losses are probable, the secondary electrons may wander through considerably greater depths (as compared to their mean free paths) before finally reaching the surface and escaping, and their energy distribution just inside the surface may be different from that at their initial generation point.

Kane[2] has presented a relatively simple one-dimensional derivation of a rate equation which includes the combined effects of the large electron-electron (or electron-hole) energy losses and of the small electron-phonon energy losses. His one-dimensional approximation for a rate equation has been shown to be a very good approximation to an exact three-dimensional random-walk description of Duckett,[3] to an exact one-dimensional solution of Langreth,[4] and to the numerical Monte Carlo calculations of Stuart, Wooten, and Spicer.[5] The one-dimensional descriptions involve the analysis of the projections of the three-dimensional path elements onto the x-direction, and consequently the characteristic parameters such as the mean free paths l_1 that appear in the one-dimensional description are related to their corresponding three-dimensional values l_3 as their averaged projections, i.e., $l_1 = l_3\langle\cos\theta\rangle$.

Using Kane's one-dimensional model approach[2] (see Fig. 3), we derive the following expression for $p(x)$, the probability that a single electron generated at depth x from the surface (with + or − x-directed velocity equally likely) will eventually strike the surface without suffering a single inelastic scattering loss that reduces the involved electron energies to values below the vacuum level energy:

$$p(x) = [c/(c+u)]e^{-ux}, \tag{12}$$

where $c = a + b$ and $U = (b^2 + ab)^{1/2}$. b is the probability per unit path length that the secondary electron will suffer a large (eliminating) energy loss either in a pair formation, or in an electron-hole recombination, and a is the probability per unit path length that a secondary electron will suffer a small energy loss as in electron-phonon scattering (generating longitudinal vibrations of the crystal lattice). The electron-electron mean free path λ_{el} and the electron-phonon mean free path λ_{pl} are equal to b^{-1} and a^{-1}, respectively. In our following Kane's approach in writing Eq. (12), we have applied his assumption that for the energy ranges involved the probabilities a and b can be considered energy independent. That this assumption is not seriously restrictive is discussed later in our relating the model results to the experimental data of interest here.

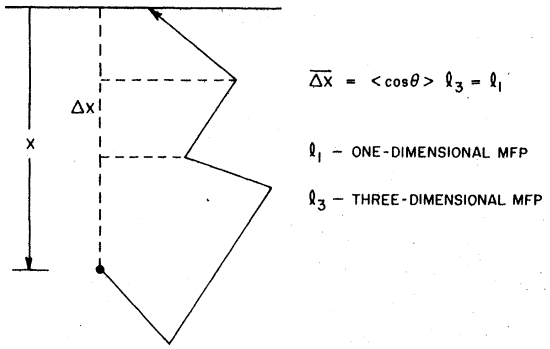

FIG. 3. One-dimensional representation of the "multiple loss" (electron-phonon) transport to the emitter surface in which the one-dimensional MFP's are the averaged projections of the three-dimensional MFP's. It is assumed that any electron-electron interaction "eliminates" the pair from the group of secondaries able to escape and that the accumulated electron-phonon energy less is simply proportional to x.

It is evident that when $b \ll a$ (insulators), the mean escape depth u^{-1}, for the random-walking electron can be very large as compared to λ_{pl}, but when $b \gg a$ (semiconductors), this mean escape depth is equal to λ_{el}.

At depth x the total number of electrons that are excited per unit area, per unit energy interval E, per unit incident photon intensity, and within a thickness dx can be written, using Eqs. (4) and (5), as

$$4\pi X(E)\,dx = 4\pi E_0 \mu(E_0) f(E_0) \rho B q(E) e^{-\alpha x}\,dx$$
$$= M(E_0) q(E) e^{-\alpha x} dx\,, \tag{13}$$

where $M(E_0)$ is a material function of the photon energy E_0 and where we have replaced $\mu\rho/\sin\phi$ by α. Using Eq. (12), the contribution to the total number of low-loss scattered electrons that strike the surface, per unit area of a semi-infinite solid, per unit photon intensity, and of energy E that have

originated within a dx thickness at x can be written

$$\frac{dN}{dA\,dE}=M(E_0)\left(\frac{c}{c+u}\right)q(E+\gamma x)e^{-(\alpha+u)x}dx\,. \quad (14)$$

In expression (14) for the contribution to the number of electrons striking the surface with energy E, we have made two important assumptions: (i) We assume that the electrons which are generated at position x and finally random walk to the surface lose an average amount of energy resulting from electron-phonon scattering that is proportional to the distance of transport, x. Ballantyne[6] has successfully applied such an assumption for secondary-electron emission as photoexcited by ultraviolet light for which the mean escape depth of the emitted electrons is essentially the mean attenuation length of the photons, α^{-1}. (This assumption is consistent with Kane's prediction that the average energy loss for all the electrons is, in fact, proportional to the average escape depth α^{-1} for large α.) For the case of x-ray excitation which is of particular interest here, the mean x-ray penetration depth α^{-1} is typically larger than the effective escape depth for those electrons that are eventually emitted. Although it is not implicit in Kane's analysis that the average energy loss in electron-phonon scattering is linearly related to the distance x for this case, Baraff[7] has shown this to be a reasonable assumption in general and independent of the initial electron energy as based upon an analysis using the Boltzmann transport equation and also upon the results of transport measurements of hot electrons in silicon as reported by Bartelink, Moll, and Meyer.[9] (ii) Our second assumption is that because of the smallness of the electron-phonon losses ($\sim 10^{-2}$ eV) and because of the relatively large penetration depths of the incident x-rays, the average number of electron-phonon scatterings that are involved before an electron finally "random walks" to the surface and escapes is sufficiently large so that the variance in its arrival energy from an average value, E, can be neglected.

In order to compare the predictions of the general relation (14) to the results for the relatively simple "no-loss" transport case treated earlier (semiclassically and three dimensionally), we let the probability for electron-phonon interactions relative to that for electron-electron interactions, a/b, approach zero so the escape depth u^{-1} approaches b^{-1} or λ_{e1} (which can be considered to be very small as compared to the mean x-ray penetration depth α^{-1}). We may then integrate Eq. (14), neglecting the effect of any multiple scattering and hence the γx term, to obtain the total number of electrons arriving just inside the surface per unit area and per unit energy interval in E to obtain

$$\frac{dN}{dA\,dE}=M(E_0)(\tfrac{1}{2})q(E)\int_0^\infty e^{-bx}dx$$

$$=\tfrac{1}{2}M(E_0)q(E)\lambda_{e1}\,. \quad (15)$$

Now if we integrate Eq. (7) in our specialized "no-loss" emission analysis to obtain the same quantity, we obtain the similar result

$$\frac{dN}{dA\,dE}=\tfrac{1}{4}M(E_0)\lambda_e q(E)\,. \quad (16)$$

Comparing Eqs. (15) and (16), we note that

$$\lambda_{e1}=\langle\cos\theta\rangle\lambda_e=\tfrac{1}{2}\lambda_e\,. \quad (17)$$

The factor $\frac{1}{2}$ corresponds to a simple averaged projection over a hemisphere for $\langle\cos\theta\rangle$. (Kane[2] and Duckett[3] have noted that the results of neutron age theory and of the three-dimensional exact random-walk analysis are in better agreement with Kane's one-dimensional model if $\langle\cos\theta\rangle$ is set equal to $1/\sqrt{3}$. In our model presentation here, however, we will use relationship (17) and a similar one that relates the electron-phonon one- and three-dimensional mean free paths, i.e., $\lambda_{p1}=\frac{1}{2}\lambda_p$.)

Because of this consistency between the one- and three-dimensional "no-loss" analyses, and because it is intuitively reasonable that we assume the distribution at the surface described by Eq. (14) to be isotropic, we proceed by comparison to the analysis as given in the development of Eqs. (7)–(11) to obtain the differential optical brightness β for photoemission which includes the mechanisms of both electron-electron and multiple-loss, electron-phonon interactions to be

$$\beta=\frac{1}{\pi}M(E_0)\frac{c}{c+u}\frac{E-E_A}{E}\int_0^\infty q(E+\gamma x)e^{-(\alpha+u)x}dx\,. \quad (18)$$

By our definition of β (following from the assumption of an isotropic distribution of secondary-electron velocities at the surface), the number of electrons emitted per unit area, per unit energy interval, and per unit solid angle is then

$$\frac{dN}{dA\,dE\,d\Omega}=I_0\beta\cos\theta\,. \quad (19)$$

Here I_0 is the photons-per-unit-area incident intensity and θ is the electron direction from the surface normal. Integrating over the half-sphere to obtain the total number of electrons emitted per unit energy interval, we have

$$\frac{dN}{dA\,dE}=\pi I_0\beta\,. \quad (20)$$

Finally, by integrating Eq. (20) over E_K $(=E-E_A)$ for the area under the emitted secondary-electron energy distribution curve (EDC) and dividing by $I_0\sin\phi$, we obtain the quantum yield Y, the number of emitted electrons per incident photon, to be

$$Y = \frac{\pi}{\sin\phi}\int_0^{E_M} \beta\, dE_K\,, \tag{21}$$

where ϕ is the angle the incident x-ray beam makes with the emitter surface and E_M is chosen here as the E_K value for which the EDC drops effectively to zero value. [$E_M = E' + E_A$, where E' is defined in Eq. (2).]

In our attempt here to develop an approximate but nevertheless complete expression for β, we need to know the E dependence of the excitation function $q(E)$ [see Eq. (18)]. As discussed earlier, this excitation function may be considered as the combined result of the secondary-electron excitation by direct electron-electron interactions with fast and with slow "primaries," and also by the promotion of secondary electrons into the conduction band utilizing the discrete energies available from plasmon deexcitation. The transition probabilities into the conduction band will, of course, be energy dependent following the density-of-states structure within the conduction band for a given emitter. For the integration of Eq. (18), however, only the "high-energy tail" of the $q(E)$ need be known, which includes the electrons of sufficient energy to eventually escape. Because the shape of the EDC's have been found to be invariant for the 0.1–10-keV photon energy region and therefore for a large range of average primary-electron energies, it seems justified to assume that the significant excitation processes can be sufficiently well described by a $q(E)$ dependence in Eq. (18) as derived for the "fast" primaries. For metals, we have successfully applied (as have Chung and Everhart[8]) the relatively "fast" electron-electron excitation function developed by Streitwolf[10] and given by

$$S(E) = P(E_p)q(E) = A/E_p(E - E_F)^2 \tag{22}$$

for metals, where E_p is the primary-electron energy and E_F is the Fermi energy. And here, for nonmetals, we similarly will adopt the excitation function derived by Hachenburg and Brauer[11] as given by

$$S(E) = P(E_P)q(E) = A'/E_P E^2 \tag{23}$$

for insulators. For both of these quantum-mechanical results, the authors assumed a free-electron-like conduction band. It is important to note that the material constants A and A' appearing here which depend upon the solid-state characteristics of the particular material (including the mass density) do *not* appear in our model equations for photoemission through the normalizing constant described earlier in Eq. (3) and defined as B. We choose $q(E)$ simply as

$$q(E) = 1/E^2 \tag{24}$$

for insulators and semiconductors, and consequently B is a dimensionless quantity.

With Eq. (24) we may now evaluate the integral in the expression (18) for β. To simplify the integral, we let $\eta = \alpha + u$, $z = (\eta/\gamma)(E + \gamma x)$, $dz = \eta\, dx$, and obtain

$$\int_0^\infty \frac{e^{-\eta x}\,dx}{(E+\gamma x)^2} = \left(\frac{\eta}{\gamma^2}\right)\left\{e^{\eta E/\gamma}\int_{\eta E/\gamma}^\infty \frac{e^{-z}}{z^2}\,dz\right\}$$

$$= \left(\frac{\eta}{\gamma^2}\right) I\left(\frac{\eta E}{\gamma}\right).$$

The integral appearing here has been accurately approximated in polynomial form in the Natl. Bur. Stand. *Handbook of Mathematical Functions*,[12] which has permitted us to evaluate $I(\eta E/\gamma)$. This function is approximately power law as shown in the log-log plot of Fig. 4 for a range in $(\eta E/\gamma)$ of 1–100. The variable $(\eta E/\gamma)$ may be interpreted as the electron's energy relative to an average accumulated electron-phonon scattering energy loss for all the electrons that random walk to the surface without an eliminating electron-electron-type collision. (This is because γ is the energy loss per unit of x and η^{-1} is an average escape depth along x.) For a given range in photoemitted energy, we might approximate the function $I(\eta E/\gamma)$ by

$$I\,\frac{\eta E}{\gamma} \approx \frac{A''}{(\eta E/\gamma)^n}\,, \tag{25}$$

and then the differential optical brightness function β becomes

$$\beta = \frac{M(E_0)}{\pi}\,\frac{c}{\eta(c+u)}\left(\frac{\gamma}{\eta}\right)^{n-2}\frac{A''E_K}{(E_K+E_A)^{n+1}}\,. \tag{26}$$

Also shown in Fig. 4 is the function $I(\eta E/\gamma)$ for

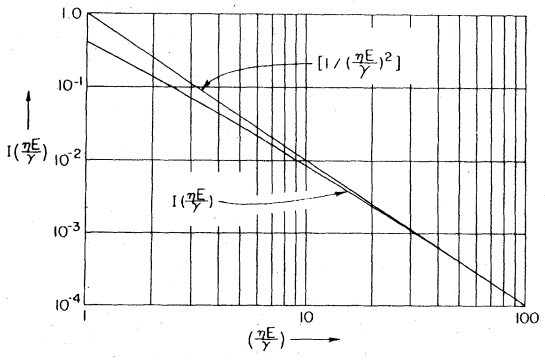

FIG. 4. Integral in the model expression (18) for β, plotted as a function of the dimensionless parameter $\eta E/\gamma$ the ratio of the arrival energy E at the surface to the mean accumulated electron-phonon loss energy. Based upon measured escape depth data, this ratio is typically greater than 10. Here, as a first approximation, $I(\eta E/\gamma)$ is set equal to the asymptotic function, $(\eta E/\gamma)^{-2}$.

the limiting "no-loss" (negligible inelastic random walking) semiconductor case with $n=2$. The relatively small departure of this function even for cases of large average electron-phonon losses ($\eta E/\gamma < 10$) suggests that the general features of the EDC under our averaging assumption of a free-electron conduction-band description are insensitive in first-order approximation to the amount of electron-phonon multiple interactions. This type of insensitivity was also noted for the case of photoemission from metals, as suggested by first-order results of cascading in the solution of the Boltzmann transport equation.[1,10]

Assuming that $n=2$ and that the x-ray penetration depths to be large as compared with the electron escape depths ($\eta \approx u$), the differential electron optical brightness β given in Eq. (26) reduces simply to

$$\beta = \frac{M(E_0)}{\pi(b+u)} \frac{E_K}{(E_K+E_A)^3}. \tag{27}$$

3. *Effect of the energy dependence of the mean free paths upon optical brightness and yield*

Anticipating that $b/a \gg 1$ for semiconductors, Eq. (27) may be rewritten

$$\beta = \frac{M(E_0)\lambda_e}{4\pi[1+\frac{1}{2}(\sqrt{1+(\lambda_e/\lambda_p)}-1)]} \frac{E_K}{(E_K+E_A)^3}. \tag{28}$$

Here we have written the b^{-1} term [the one-dimensional electron-electron mean free path (MFP)] as equal to one-half the three-dimensional MFP value λ_e. The small amount of "random walking" allowed here results in the additional term $\frac{1}{2}[(1+\lambda_e/\lambda_p)^{1/2}-1]$. In this correction term we may use average values of the MFP's to be consistent with the Kane rate-equation analysis assumption of these parameters being energy independent. Neglecting this term reduces Eq. (28) immediately to the simple "no-loss" result, as discussed earlier, and given in Eq. (11). For this case, the factor λ_e (the three-dimensional electron-electron MFP) is a "no-loss" effect and should be written with its full energy dependence.

The probability per second for electron-electron scattering as based upon a simple energy fold over electron density-of-state functions has been calculated by Kane,[12] which is in accord with an earlier derivation by Berglund and Spicer[13] as based upon energy consideration alone. Using this model for the simple case of free-electron bands, Schwentner[14] has calculated the MFP, λ_e, for electron-electron scattering (as well as for electron-hole scattering) to be

$$\lambda_e = KE^{1/2}/(E-E'_G)^2. \tag{29}$$

[It is assumed that the probability rate, or inverse lifetime, is simply proportional to the number of states available in the conduction band to the recoil and to the excited electrons in pair production, and therefore to $\rho(E')\rho(E-E'-E_G)$. $\rho(E)$ is the conduction-band density of states, E is the electron energy, E' its final-state energy, and $E-E'-E_G$ is the energy of the promoted valence electron. Integrating over all possible states in E', the total probability, or $1/\tau$, for an "averaging" free-electron parabolic conduction-band density of states ($\rho(E) \sim \sqrt{E}$) becomes

$$P(E) \sim \int_0^{E-E_G} \rho(E')\rho(E-E'-E_G)\,dE'$$

and

$$1/\tau = \int_0^{E-E_G} [E'(E-E'-E_G]^{1/2}\,dE' \sim (E-E_G)^2.$$

Letting the MFP, $\lambda_e = v\tau$, and the electron group velocity v be proportional to $\sqrt{E}$, we obtain the expression given in Eq. (29).] We may now present a complete expression for β for *semiconductors* as follows:

$$\beta = \frac{KM(E_0)}{4\pi[1+\frac{1}{2}(\sqrt{1+\lambda_e/\lambda_p}-1)]} \frac{E_K}{(E_K+E_A-E'_G)^2(E_K+E_A)^{5/2}}, \tag{30}$$

where $\mu(E)$ is given by Eq. (13).

We have plotted the energy dependence of Eq. (30) for several values of E'_G/E_A in Fig. 5. (It should be noted as in Fig. 1 that the energy-gap value, E'_G, which appears here properly is measured to that point where pair-production begins.) For this semiconductor relation (30), it follows that the electron energy E_{KP} at the peak may be approximated as

$$E_{KP} \approx E_A[0.280 - 0.077\,(E'_G/E_A) - 0.156(E'_G/E_A)^2], \tag{31}$$

and the full width at half maximum of the EDC, Δ, may be approximated as

$$\Delta \approx E_A(0.90 - 0.26(E_G/E_A) - 0.45(E_G/E_A)^2). \tag{32}$$

This FWHM value, Δ, thus is predicted to decrease with E_A and as E_G/E_A approaches unity. And finally, using Eq. (21), we derive the expression for the semiconductor secondary-electron yield Y to be

$$Y = \frac{0.13KM(E_0)\exp[2.1(E'_G/E_A)^2]}{2\{1+[1+(\lambda_e/\lambda_p)]^{1/2}\}E_A^{5/2}\sin\phi}. \tag{33}$$

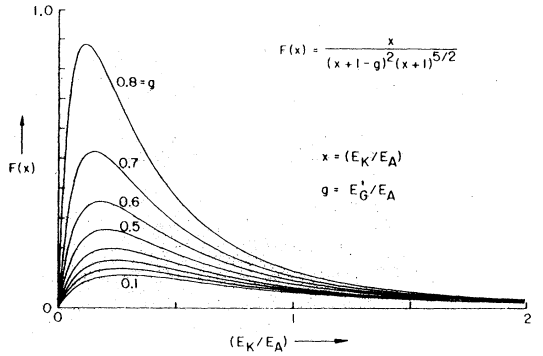

FIG. 5. Predicted E_K dependence for semiconductors for which the electron-electron scattering probability is large compared with that for electron-phonon scattering. Suggested here is that the FWHM of the EDC is proportional to E_A and decreases as E_G/E_A approaches unity.

(Here we have numerically determined the integral

$$\int_0^{20} \frac{x\,dx}{(x+1-g)^2(x+1)^{5/2}} \approx 0.13 \exp(2.1\, g^2)\,,$$

where $x = E_K/E_A$ and $g = E_G/E_A$.)

For many *insulators* (as defined here), the probability for electron-electron scattering relative to that for electron-phonon scattering is very small. In this case, $(b/a \ll 1)$ and again we shall assume that the x-ray penetration depths are large as compared to the electron escape depths, i.e., $\alpha \ll u$. We shall also choose to approximate the function $I(\eta E/\gamma)$ by $1/(\eta E/\gamma)^2$, as we have expressed in Eq. (27). (It is suggested by the measured escape lengths for the alkali halides,[15] for example, that this function is well approximated by a power to $n = 2$.) We therefore may rewrite Eq. (27) for the differential electron optical brightness β for *insulators* as

$$\beta = \frac{M(E_0)}{2\pi} \frac{(\lambda'_e \lambda_p)^{1/2}}{[(1+\lambda_p/\lambda'_e)^{1/2} + (\lambda_p/\lambda'_e)^{1/2}]} \frac{E_K}{(E_K + E_A)^3}\,, \tag{34}$$

where $M(E_0)$ is given by Eq. (13).

For the insulator case, we introduce here a small probability, b', for an "eliminating" pair production which is equal to $1/\lambda'_{e1}$ and which may be the result of an energetically possible ionization of impurity atoms, for example, within the real sample. Without such a mechanism for relatively large losses, the escape length, $(b'^2 + ab')^{1/2}$, as predicted by the Kane rate equation[2] would seem to predict excessively large escape depths not reconcilable by incorporating the finite electron-phonon losses and not consistent with measured depths for materials for which valence-band electron interactions are not energetically permitted (insulators). Again we have expressed the one-dimensional MFP values a^{-1} and b'^{-1} by their equivalent three-dimensional values $\frac{1}{2}\lambda_p$ and $\frac{1}{2}\lambda'_e$, respectively.

The MFP λ_p has been the subject of theoretical treatment by several authors. Garwin and Llacer[16] derive an expression for $\lambda_p(E)$ which is approximately proportional to E. Wooten[17] reviews this topic and concludes that in general it is reasonable to assume that $\lambda_p(E)$ for $E \gg E_p$ be regarded as constant, where E_p is an average electron-phonon interaction loss energy. This is consistent with the result given by Herring[18] and Conwell.[19] (For a review of such treatments, see Ref. 20.) They have given λ_p as

$$\lambda_p = \lambda_0 \tanh \frac{E_p}{2kT}\,, \tag{35}$$

where λ_0 is the high-energy low-temperature (T) asymptote of the MFP. Equation (35) suggests that for a particular insulator at a given temperature, λ_p may be considered a constant, as we have assumed in fillowing Kane's one-dimensional development of a rate equation. In Eq. (34) for the small λ_p/λ'_e ratios, we may use simply an average value for the λ'_e. Because of the relatively small energy range involved in the EDC's of the insulators studied and presented here and because of the appearance of λ'_e to the one-half power in the $(\lambda'_e\lambda_p)^{1/2}$ factor in Eq. (34), it seems justifiable to allow the λ'_e value here also to be its average value and thus energy independent. For this insulator model relation (34), it then follows that the electron energy E_{KP} at the peak intensity position of the EDC is given by

$$E_{KP} = \tfrac{1}{2} E_A\,, \tag{36}$$

and that the full width at half maximum Δ of the EDC is

$$\Delta = 1.90\, E_A\,. \tag{37}$$

Finally, using Eq. (21), we derive an expression for the secondary-electron yield Y to be

$$Y = \frac{M(E_0)}{4E_A \sin\phi} \frac{(\lambda'_e \lambda_p)^{1/2}}{[(1+\lambda_p/\lambda'_e)^{1/2} + (\lambda_p/\lambda'_e)^{1/2}]}\,. \tag{38}$$

In our derivations of the above expressions (34) for β and (38) for Y for insulators, we have not taken into account the enhancement of the photoemission by the effect of internally reflected electrons which may random walk back to the surface and possibly escape. Duckett[3] has derived such an enhancement factor which may be written

$$F = 1/(1 - R\{1 - [b'/(a+b')]^{1/2}\}^2) \tag{39}$$

by which our β and Y values for insulators could be multiplied. An effective value for an average internal reflection coefficient, R, may be defined in terms of an average escape cone solid angle Ω

by the quantity $(2\pi - \Omega)/2\pi$. If we insert a value of Ω corresponding to an electron energy E using the escape cone angle θ_c' as defined earlier, a value for $R(E)$ becomes simply $(E_A/E)^{1/2}$. For a real insulator for which the internal reflection may be small and diffuse, and for which $b' \simeq a$ (as deduced from measured escape depths), the enhancement factor F is considered as effectively constant and approximately equal to unity.

III. EXPERIMENTAL MEASUREMENTS AND RESULTS

A. Measurement procedure

The semiconductor and insulator materials that are studied here were vacuum evaporated from tungsten or molybdenum "boats" loaded with sufficient high-purity powdered samples to deposit approximately 3000-Å thick films onto microscope slide substrates that were coated with a vacuum evaporated conducting layer of gold. These samples were transferred in dry nitrogen to an eight-position sample holder of the electron spectrometer and 10^{-8}-Torr environment. A schematic of the x-ray source-sample holder-hemispherical electrostatic analyzer spectrographic system is shown in Fig. 6. A uniform field acceleration allowed a precise correction for the electron optical brightness as measured by the spectrograph in order to obtain a value for β at the emitter surface. The details of the electron optics and brightness correction have been presented in an earlier paper.[1] It may be readily shown that

$$d = 2(l + h)\tan\phi \,, \tag{40}$$

where d is the effective sample diameter. This limiting sample diameter as "seen" by the spectrometer in these measurements was 9.3 mm ($l = 109$ mm, $h = 10$ mm, and $\phi = 2.24°$). The theoretical and measured energy resolution of the spectrometer for these measurements was approximately 0.03 eV. An x-ray source of Al-$K\alpha_{1,2}$ (1487 eV) was used in the measurements as obtained with 6-μ aluminum foil filtering[21] of the radiation from an aluminum anode at 4 k. Such a source presents somewhat more than 95% Al-$K\alpha$ radiation with most of the approximately 4% continuum background centered around 2500 eV.

The experimental measurements were made on two sets of samples, each set prepared independently (usually on different days). The secondary-emission data from the spectrograph was corrected for the brightness change due to the acceleration and plotted as n/n_p vs E_K using a small laboratory computer-plotter system. (n is the electron counts per data point divided by the collection time and the x-ray source current. The

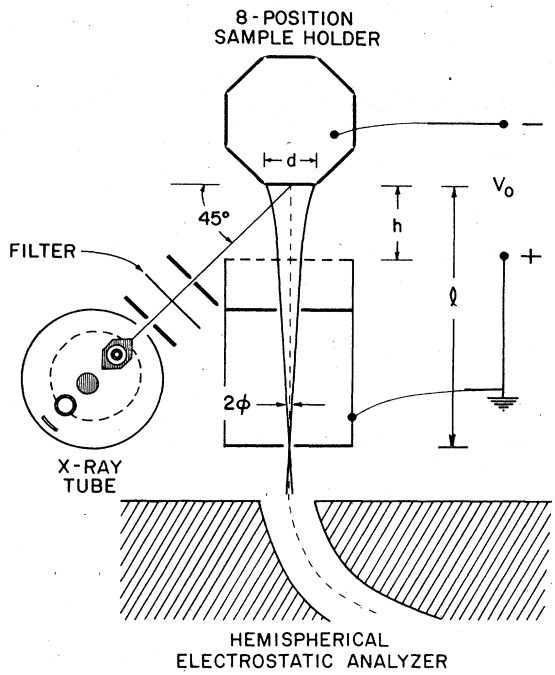

FIG. 6. Six-μ aluminum foil filtered Al-$K\alpha$ (1487 eV) photons were used to excite the EDC spectra shown in Figs. 8-13. The hemispherical energy analyzer was set to accept 15-eV electrons, with a beam solid angle defined to yield 0.01-eV energy resolution. A uniform preacceleration field was employed which permits a simple and precise brightness correction. The accelerating potential is step scanned. A multiple sample holder allows an immediate relative spectral measurement on several samples and a gold standard.

normalizing value n_p is this value at the peak of the EDC.) These curves reproduced among the sample sets within about 1% average deviation.

In order to minimize any effect of instrumental drift or other causes that might affect the spectrometer transmission, each measured EDC of a given sample was immediately followed by a similar measurement of an EDC of two relatively stable "standard" samples: gold and copper iodide.

In order to determine the differential electron optical brightness β from the n/n_p data for the sample and standard, we introduce an overall instrument calibration constant K' by the relation

$$\beta = K' n \,. \tag{41}$$

Then from Eq. (21) we may write for the secondary-electron yield Y

$$Y = \frac{\pi K'}{\sin\phi} \int_0^{E_M} n \, dE_K = \frac{Y_0}{\sin\phi} \tag{42}$$

so that

$$K' = Y_0/\pi\sigma \,. \tag{43}$$

The area under the experimental EDC, σ, is obtained by numerical integration as the EDC is plotted. By applying Eq. (42) to establish the instrumental constant K' from data related to the standard sample, we may obtain the relationship between the differential brightness β and the normalized n/n_p EDC experimental curve:

$$\beta = (Y_{0s} n_{ps}/\pi\sigma_s) p (n/n_p) = a(n/n_p) , \quad (44)$$

$$a = Y_{0s}(n_{ps}/\pi\sigma_s)p ,$$

where n_{ps} and σ_s have been measured on the standard sample of a known yield value, Y_{0s}, and the ratio p is the intensity n_p as measured at the peak position of the sample EDC relative to that, n_{ps}, as measured under identical conditions on the standard sample. The experimental EDC's that are presented here are normalized (n/n_p) curves and thus equivalent to β/a curves.

B. Experimental secondary-electron energy distributions

These EDC data are presented as the experimental point plots along with the experimentally determined values for the electron kinetic energy at the peak intensity position E_{KP}, the full width at half maximum Δ, and the peak intensity and the yield relative to these values as measured for the gold photocathode standard under identical photon excitation p and y, respectively. A typical measured EDC for the gold standard sample is shown in Fig. 7 (Ref. 22). Band-gap values E_G are presented as obtained from the literature. The "best fitting" by the model equations as derived above are presented along with the chosen values of the electron affinity parameters, E_{A_x}, which have yielded these fits.

The absolute values for β may be obtained from these β/a curves using Eq. (44). For the gold reference sample employed for these measurements, Y_{0s} and the EDC shape parameter $n_{ps}/\pi\sigma_s$ are 0.054 and 0.064 eV^{-1}, respectively, and approximate value for a is thus equal to 3.4×10^{-3} eV^{-1}.

1. Semiconductors

The samples which are presented and defined here as "semiconductors" were those for which the emitted electrons are of energy E that is greater than the band-gap value E_G. These samples are AgCl, Se, CdS, PbS, Ge, and PbI_2, and their EDC's are presented in Figs. 8 and 9. In fitting by the theoretical curves, the semiconductor relation for β given in Eq. (28) was rewritten

$$\beta = \frac{KM(E_0)}{4\pi}\left(\frac{K}{\lambda_e}+\epsilon\right)^{-1}\frac{E_K}{(E_K+E_A)^3} , \quad (45)$$

with λ_e given by Eq. (29), and ϵ is considered essentially a constant to be adjusted for "best fitting."

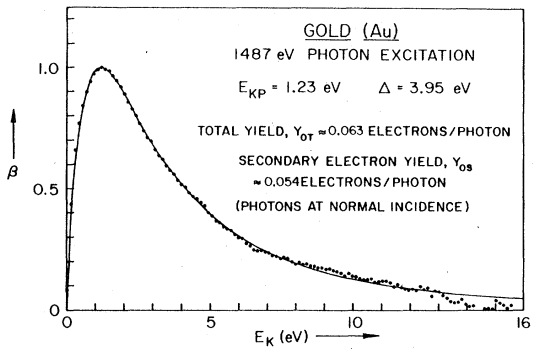

FIG. 7. EDC for gold as excited by Al-$K\alpha$ (1487 eV) photons. The smooth curve is based upon a theoretical model developed in Ref. 1 for x-ray photoemission from metals. In the present work, for the EDC measurements on semiconductors and insulators shown in Figs. 8–13, the peak heights and secondary-electron yields relative to those of a gold standard are presented as the p and y values, respectively. Given here are our preliminary measurements on the total yield and the secondary-electron yield for gold prepared by evaporation the same way as our spectrographic standard. The secondary yield was determined as the difference between the total yield and that for the fast electrons alone with the secondaries retarded by a 30-V grid potential.

Thus the electron-phonon scattering term in Eq. (28) is given by

$$\epsilon(\lambda_e/K) = \tfrac{1}{2}[(1+\lambda_e/\lambda_p)^{1/2}-1] = \epsilon E^{1/2}/(E-E_G)^2 \quad (46)$$

$$(\epsilon \approx K/4\lambda_p \text{ for } \lambda_e/\lambda_p \ll 1).$$

Relationship (46) allows an estimate of the value of the (λ_e/λ_p) ratio characteristic of the semiconductor and for a given emitted energy E. With the EDC plots we have listed the characteristic parameters for these curves. As discussed earlier, the band-gap energy E'_G that appears in Eq. (29) is defined as the separation between the mean position in the valence band and the onset position for pair-production; nevertheless, we have used the reported band-gap value[19] as measured to the bottom of the conduction band E_G in the calculation and plotting of the theoretical curves.

For the CuI photocathode, the EDC of which is shown in Fig. 10, the semiconductor relation as given in Eq. (45) cannot be used for the values of E_K less than $E_G - E_A$. Below this energy, electron-electron scattering becomes very improbable and electron-phonon scattering becomes dominant. For CuI, this occurs approximately at 1 eV, as indicated by the arrow in Fig. 10. Therefore, for the region $E < E'_G$, the relation for β as derived for insulators and given in Eq. (34) is appropriate. A composite curve was thus used in Fig. 10 by imposing a continuity condition at this 1-eV position to determine effectively the factor involving

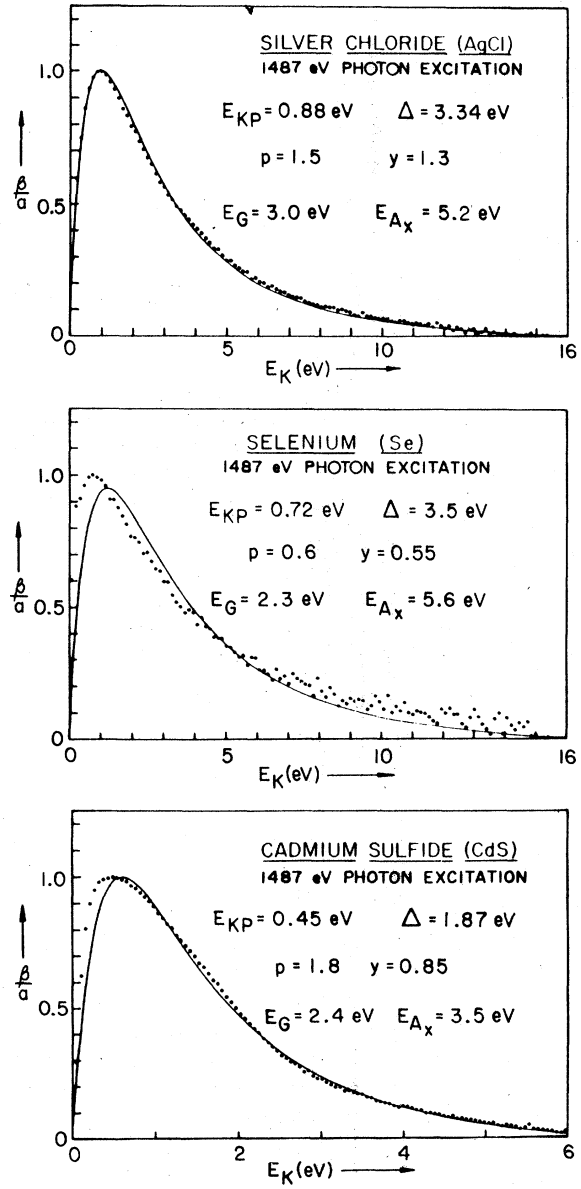

FIG. 8. Theoretical and measured EDC's for semiconductors for which $E_A > E_G$, E_{A_x} values were chosen for "best fitting" with model Eq. (45) with $\epsilon = 0$. E_{KP} and Δ are defined in Fig. 1; p and Y are peak and yield values relative to those measured under identical conditions for gold. For these EDC's (measured relative to gold) the constant a as given by Eq. (44) is approximately equal to $(3.4\times10^{-3})P$ eV^{-1}. E_G values are taken from the literature (see, for example, Ref. 19).

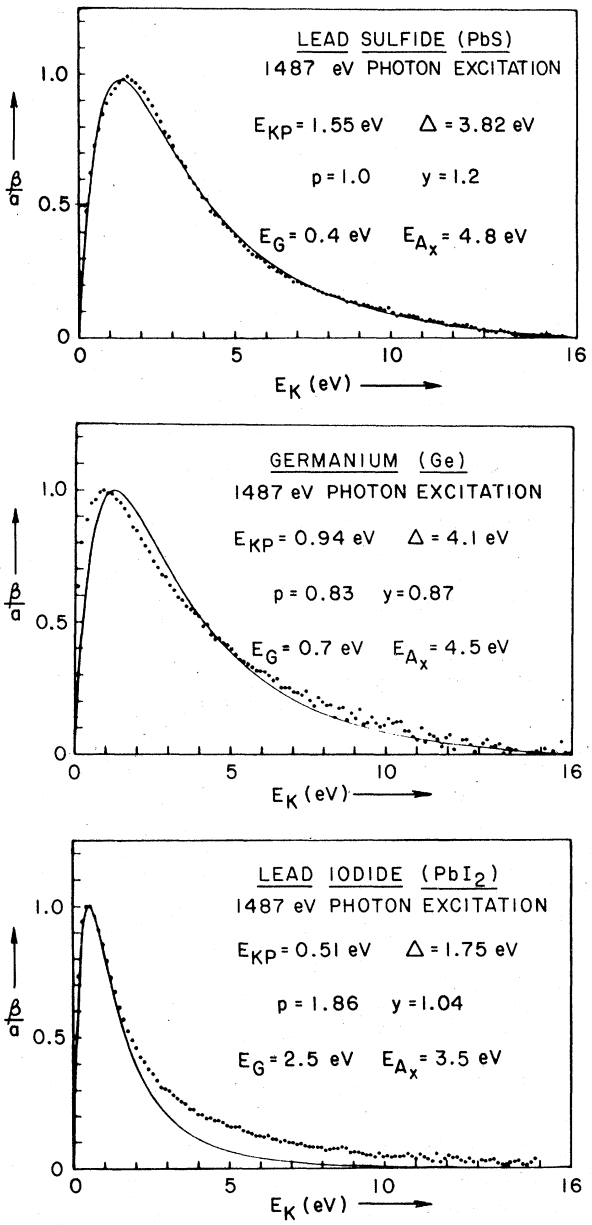

FIG. 9. See caption for Fig. 8.

λ_e' and λ_p appearing in Eq. (34). It is interesting to note that a "kink" appears in the experimental data at this critical energy position.

As has been illustrated in Figs. 8, 9, and 10, the experimental and the theoretical curves are generally in good agreement.

2. *Insulators*

The samples which are presented and defined here as "insulators" are chosen among the alkali halides and have band-gap energy values that are greater than the energies E of the emitted electrons. For these samples, the electron-phonon scattering process is dominant and some of their EDC's show strong structural features. In our presentation of a model EDC expression (34) for the insulators, we were required to use constant or "average" values for the appropriate MFP values and an excitation function based upon an "aver-

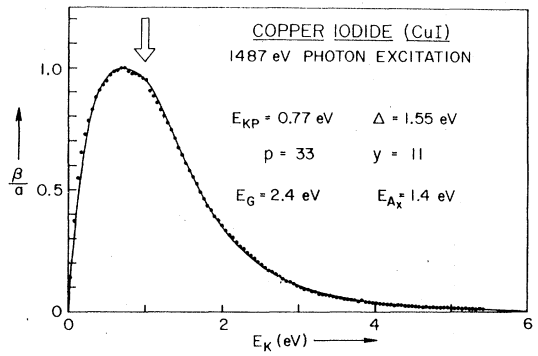

FIG. 10. For copper iodide, the emitted electrons of E_K less than approximately 1 eV would have insufficient energy to interact with the valence electrons in promoting these to the conduction band. Therefore, a fit with Eq. (45) for semiconductors was used only for the region above 1 eV and for best fitting ϵ was determined to be equal to 0.71. Below this point, the EDC was fit, with a continuity conditon, to the model expression (34) for insulators.

aging" free-electron band-structure description. We have chosen E_A values in fitting Eq. (34) to the experimental data that present curves which approximately average through the EDC structure and thus have a similar areas and predicted yields.

In Figs. 11, 12, and 13 are shown the EDC's for the alkali halides LiF, NaCl, KCl, KBr, RbBr, NaI, KI, RbI, and CsI. Presented here also are the values for the measured E_{KP}, Δ, and the peak intensity and yield relative to these values for gold, p and y. The given values for E_{A_x} were those chosen for the "best-fit" -curves according to Eq. (34). The characteristic parameters for the EDC's of these alkali halides are listed along with the EDC plots.

IV. STRUCTURAL FEATURES OF THE EDC's

In view of the reasonably good agreement between the observed EDC's (Figs. 8, 9, and 10) and Eq. (45), as derived in Sec. III for the *semiconductor* samples, considerations of structural features of these EDC's will be left to remarks which have already been made concerning CuI. This was the only semiconductor sample for which any noticeable spectral structure was observed. The situation for the insulators (alkali halides), on the other hand, is quite different; we shall now attempt to explain many of the features observed in the spectra of Figs. 11, 12, and 13 in terms of the electron energy-band structures and characteristic electron energy-loss data for these solids.

A review of band-structure calculations which have been performed for many of the alkali halides may be found in Ref. 23. For some halides, many

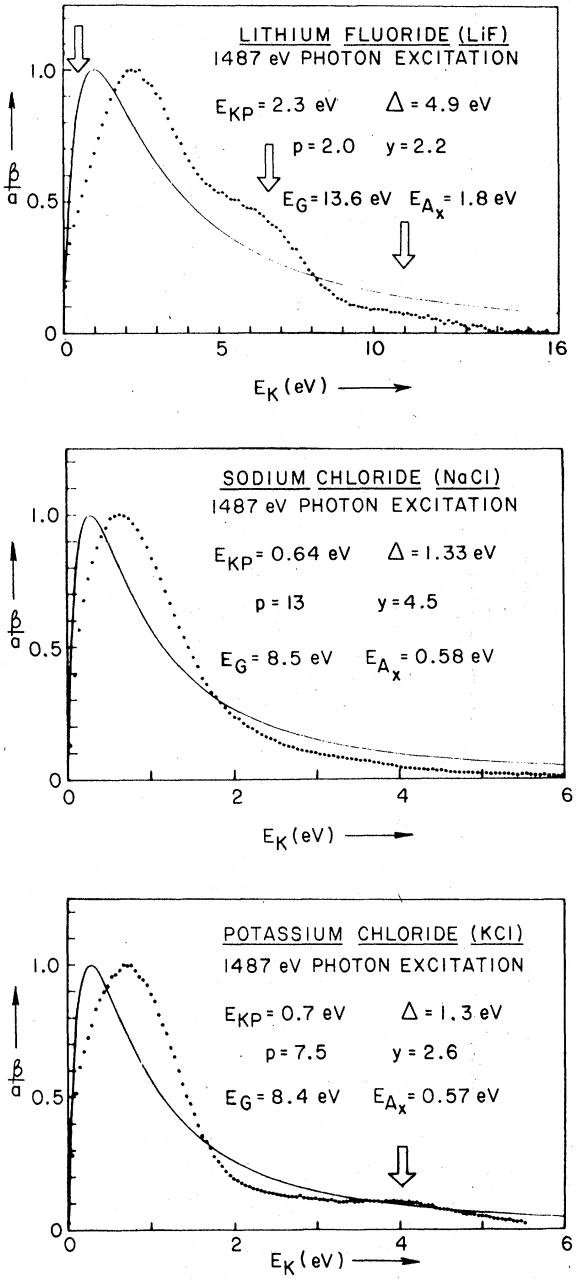

FIG. 11. For the alkali halides presented here and in Figs. 12 and 13, the energy of the emitted electrons would have been insufficient for interacting with the valence electrons in pair production and hence these are classified here as insulators. The E_{Ax} values were chosen in fitting the model expression (34) for insulators so as to have approximately the same area under the curve (yield) as for the experimental curve. This fitting criterion is somewhat arbitrary, and it is proposed here that superimposed on the model prediction for the EDC is, in some insulators, the plasmon deexcitation structure. See Fig. 8 caption for the value of the normalizing constant, a. The E_G values cited in Figs. 11, 12, and 13 are from Ref. 23.

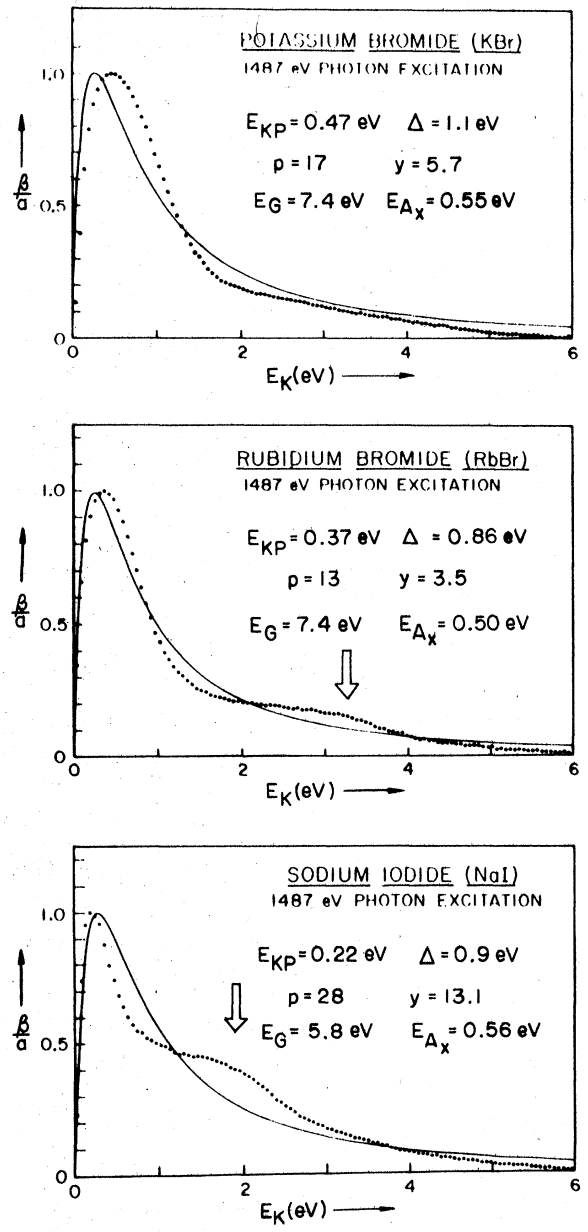

FIG. 12. See caption for Fig. 11.

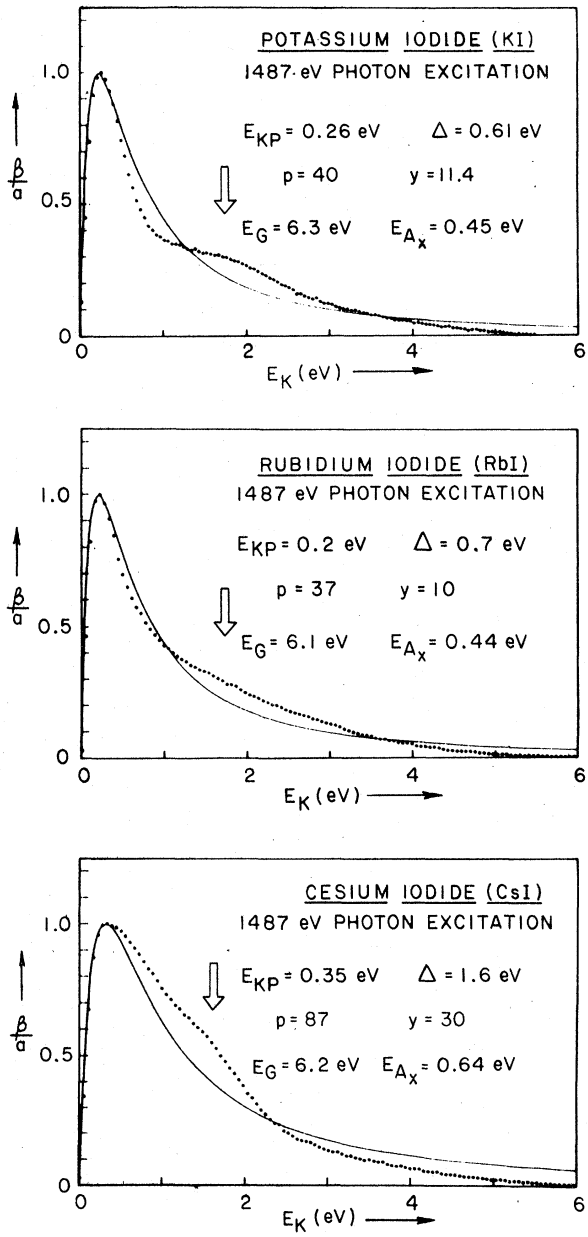

FIG. 13. See caption for Fig. 11.

calculations have been made, while for others relatively few or none have been published. The band calculations which are referred to in what follows have been selected on the grounds that they have produced values of E_G (either from first principles or by *ab initio* fitting) and E_A. In this regard, it is worth noting that band calculations employing a local approximation (Slater exchange) to the exchange potential produce very poor comparison with experimentally determined E_G and E_A values and valence-band-width values. Hartree-Fock methods incorporating correlation effects such as have been used by Kunz, Lipari, and Fowler (see references contained in Ref. 23) seem to produce parameters in good agreement with the same experimental quantities for several of the alkali halides.

It is also now well known that in insulators such as the alkali halides, it is possible to produce concurrently both exciton and plasmon excitations.[24,25] Later in this section we shall show that in fact most of the predominant x-ray excited EDC struc-

tural features can collectively be shown to exhibit good agreement with plasmon energy losses.

We shall first, however, consider the structural features of the EDC's in terms of comparison with results obtained by other workers and in terms of calculated band structures and densities of states.

A. Lithium fluoride

The main structural feature in the EDC is near $E_K = 6.7$ eV (see arrows in Fig. 11 and in other figures when being referred to structure in the EDC's). Other smaller structures may be seen at $E_K \sim 0.5$ eV. The lower-energy region of the LiF conduction band is derived from orbitals with the character of Li $2s$, Li $2p$, and F $3d$ states. Menzel *et al.*[26] have shown that the conduction-band density of states (DOS) has peaks at 13.3, 18, and 22.3 eV above the conduction-band minimum at Γ_1. In the present case, this would correspond to peaks at $E_K = 1.46$, 6.1, and 10.4 eV, in fair agreement with the observations presented above, although in terms of peak intensities the agreement is poor. Similarly, inspection of the calculation by Page and Hugh[27] would seem to indicate a combined s-d peak in the density of states at $E \sim 9.9$ eV, i.e., at $E_K \sim 7$ eV.

Ultraviolet photoelectron emission[28] and synchrotron final-state spectroscopy[29] indicate features attributed to conduction-band DOS peaks at $E_K = 3.3$ and 7.8 eV and at 15.2 and 19.6 eV above the valence band, respectively. These are not resolved in the present work, but the peak at 15.2 would imply a high density of states near the bottom of the conduction band.

A possible mechanism for the observed $E_K = 6.7$ eV peak may be considered via KVV Auger excitation. The mean intervalence band separation in LiF is ~50 eV so that a valence-band (V) Auger electron is characterized by $E_K = 50 - 11.8 = 38.2$ eV.[28] If such electrons were sequentially to lose energy both by pair production (13.6 eV) and by a characteristic energy loss[24] of 18.3 eV (interband transition), they would have residual $E_K = 6.3$ eV. This is in the region of the structure observed.

As indicated later, however, a more likely explanation for this structure is via plasmon deexcitation.

B. Sodium chloride

Similarly to LiF, the d-like conduction bands in NaCl are associated with the anion. Although there appear to be no structural features in the secondary distribution, Lipari and Kunz[30] have derived a conduction band DOS with peaks at 4 and 6.5 eV above the minimum at Γ. These would correspond here to $E_K = 3.5$ and 6 eV and are not discernable.

Characteristic energy losses for electrons in NaCl have, however, been observed by Battye *et al.*[31] and Cruezberg[32] with values of 9.6 and 10.1 eV, respectively. With $E_G + E_A = 8.95$ eV, this would simply imply a peak in the EDC at ~1 eV. This would account for the observed anomalously high peak in the EDC relative to the theoretical curve in Fig. 11.

Peaks attributed to conduction-band DOS structure have been measured by Pong and Smith[33] using ultraviolet photoemission spectroscopy (UPS), and are placed at $E_K = 2.0$ (weak) and 3.5 eV. Using a photon energy of 21.2 eV, however, they do not observe these features in the secondary-electron "tail" which has a span of $E_K = 0 \rightarrow 4$ eV. This agrees well with the present work.

C. Potassium chloride

For this sample, there is considerable overlap of the d- and s-like bands. Contrary to the previous two samples, however, the d-like orbitals derive from orbitals on the cation. Band-structure details as determined by Lipari and Kunz[34] indicate a high DOS contribution from the d bands at Γ_{25} and near the X_3 minimum, which are 5.55 and 1.87 eV above the conduction-band edge at Γ_1. These correspond to $E_K = 5$ and 1.37 eV, respectively. Final-state spectroscopy measurements using synchrotron radiation[35] also indicate high DOS in the conduction band at 9.7 and 12.6 eV above the valence-band maximum, i.e., at $E_K = 0.8$ and 3.7 eV. The lower value would account for disagreement between the observed EDC and the theoretical curve in Fig. 11, while the higher value is in the region of the structure arrowed in Fig. 11 at 4 eV.

Further confirmation of this is given by Pong and Smith,[36] who have found DOS structures at $E_K = 1.3$ and 4.5 eV using UPS.

D. Potassium bromide

It is well known that the band structures of KBr and KCl are very similar.[37] This is also noticeable in the similarity of the secondary EDC's for these samples. Qualitatively, then, we apply the same arguments as above and simply add that Pong and Inouye[38] recently have observed structures attributable to conduction-band DOS peaks at $E_K = 0.9$ and 3.8 eV.

E. Rubidium bromide

The band structure for RbBr is similar to that for KBr.[39] Inouye and Pong[40] have measured DOS peaks at $E_K = 1.0$ and 3.4 eV, the latter peak agreeing well with the arrowed structure in Fig. 12, and

the former peak possibly causing the above-mentioned enhancement of the main EDC peak in relation to the theoretically predicted curve.

F. Alkali iodides (NaI, KI, RbI, CsI)

The structure of the conduction band in Li and Na halides is relatively simple compared with K, Rb, and Cs halides in that Li^+ and Na^+ have no low-lying d states. The K, Rb, and Cs halide exhibit strong alkali d character in the conduction band, and this feature occurs most strongly for the iodides in that for these solids, the d overlap with the lowest-lying s band is greatest for the iodides.[41-44] Furthermore, the d states lower as the atomic number of the alkali ion increases.

The EDC for NaI (Fig. 12) shows structure indicated by the arrow at 1.0 eV. This may be associated with d states well separated from the low-lying s states, along with a similar feature observed in UPS by Pong and Inouye[38] for NaI, and so may be identified with structure in the conduction-band DOS. These authors observed a peak at $E_K = 1.5$ eV.

In KI, RbI, and CsI there appear to be features attributable to low-lying d-band DOS at $E_K = 1.8$, 1.7, and 1.6 eV, respectively. The decreasing values of E_K are consistent with the d-band lowering with increasing atomic number of the alkali ions. In a detailed comparison with band-structure results, it may be seen that for KI (Refs. 41 and 37) there is evidence for a region of high DOS at $E_K = 1.8$ and 2.3 eV, respectively, in good agreement with Fig. 13. For RbI (Ref. 42), similar DOS structure would seem to exist at $E_K \sim 3$ eV which is in fair agreement with the observations. Further experimental confirmation of the structure observed here ($E_K = 1.7$ eV) for RbI is found in the UPS observation[40] that RbI shows conduction-band structure at $E_K = 1.8$ eV. Finally, for CsI, which shows EDC structure at $E_K = 1.6$ eV (Fig. 13), it may be noted that this is in excellent agreement with UPS measured structure[45] at $E_K = 1.7$ eV, and in fair agreement with high $5d$-like DOS at $E_K \sim 2$ eV in the band-structure calculation of Onodera.[44]

We now turn to considerations involving the possible presence in the observed EDC's of structure due to plasmon energy losses. Observed plasmon losses from both electron and optical absorption experiments have been compared with theoretical plasmon energy estimates for the alkali halides in Refs. 24 and 46, and are summarized in Table I. If one were tentatively to assume that such plasmons lose their energy to single electrons in the valence band, then it might be expected that the observed EDC's would show plasmon loss structures at $E_{KS} \sim \hbar\omega_p - E_G - E_A - \Delta E_V$, where ΔE_V is the valence-band half-band width.[23] These quantities are given in Table I. A comparison of the last two columns of Table I may then be seen to result in reasonable agreement (within the present indeterminancy of the E_a and E_A values) between the predominant EDC structures and the plasmon loss mechanism.

The plasmon energy-loss observation by other workers alluded to above are in many cases the strongest energy-loss features in the characteristic energy-loss spectra of the alkali halides.[46-48] While it has been shown that some of the structures presented here may be approximately identified with interband transitions and conduction-band densities-of-states effects, we tentatively favor the explanation for the predominant EDC structures in terms of plasmon energy losses since these

TABLE I. Alkali halide EDC structures.

Sample	$\hbar\omega_p$ (eV)[b]	E_G (eV)[a]	E_A (eV)[a]	ΔE_V (eV)[a]	Plasmon predicted sturcture (eV) (±0.5) $\hbar\omega_p - E_G - E_A - \Delta E_V$	E_K (eV) observed EDC features (±0.1 eV)
LiF	25.3	13.6	1	3.7	7	6.7
NaCl	15.5	8.5	0.4	2.2	4.4, 0.3	···
KCl	14.0	8.4	0.4	1.5	3.7	4.0
KBr	13.5	7.4	0.8	1.4	3.9	···
RbBr	12.3	7.4	0.4	1.6	2.9	3.2
NaI	13.3	5.8	1.5	3.3[c]	2.7	1.9
KI	11.4	6.3	1.2	2.4	1.5	1.75
RbI	11.1	6.1	1.1	2.1	1.8	1.7
CsI	10.7	6.2	0.2	2.3	2.0	1.6

[a] Reference 23.
[b] References 24 and 46.
[c] Reference 39.

processes would seem to predict better overall agreement, as may be seen from Table I.

Two samples (LiF and RbI), both of which show significant EDC structure, were reexamined using $CK\alpha$ x-rays (277 eV) and Cu-$K\alpha$ (8050 eV). The EDC shapes remained substantially the same as those shown in Figs. 11 and 13 and as excited by using Al-$K\alpha$ (1487 eV). The implication is that the direct excitation of secondary electrons and the indirect process of first generating plasmons which deexcite to generate secondary electrons both have a similar dependence upon the primary electron energy and hence upon the exciting photon energy.[49] This result was anticipated in our model assumptions, as discussed earlier and expressed in Eq. (1).

V. CONCLUSIONS

An experimental method has been demonstrated for precisely measuring the secondary-electron EDC's and the relative secondary-electron yields for dielectric films in the 0.3-μ thickness range as vacuum evaporated upon conducting substrates. Although for this study the samples were prepared outside the spectrograph, the measured EDC's were found to be reproducible and for many with such strong characteristic differences that it is believed that the EDC's are fairly representative of "clean" samples and accurately representative of typical photocathodes as prepared for x-ray detectors, streak, and framing cameras.

A simple theoretical model has been developed which takes into account strong electron-electron and weak electron-phonon losses in the secondary-electron transport within the emitter. In first approximation, this model predicts that the secondary-electron energy distribution for insulators has a dependence upon the electron energy E as is given by the product of the internal excitation function $q(E)$ and the excape factor $(E - E_A)/E$. For the semiconductors, an additional factor must be included that is equal to $\lambda_e(E)$, an energy-dependent MFP for electron-electron scattering. The $q(E)$ function [see Eq. (1)] is assumed to be a sum of the contributions resulting from secondary-electron excitation by direct primary-electron interaction, $q_F(E)$ and $q_S(E)$, and by plasmon deexcitation $q_P(E)$. Here we have further assumed that the direct excitation process can be considered as dominant and that correspondingly $q(E)$ can have an E^{-2} dependence, as derived from a simple free-electron conduction-band model. Any DOS and plasmon deexcitation structural detail has been considered as superimposed upon this averaged EDC description.

As has been shown in the EDC's for the semiconductors presented in Figs. 8, 9, and 10, the fitting of the model curves to the experimental data is very satisfactory. Strong DOS structure is not present for these semiconductors and no strong plasmon deexcitation structures appear in these semiconductor EDC's because the observed secondary electrons have energies as measured from the valence band that are less than that of the expected strong plasmon excitations (of the order of 10–20 eV).

However, as shown for many of the alkali halide EDC's presented in Figs. 11, 12, and 13, structural features have been found which can be reasonably well correlated with plasmon deexcitations to single secondary electrons that have energies within the main EDC energy region. We have noted that these structural features can, in many instances, be also correlated with published DOS peaks and interband transitions. Nevertheless, the initial primary electrons that are generated under x-ray excitation lose an appreciable function of their energy first to plasmon excitations. The plasmon peaks dominate the characteristic energy-loss spectra of the alkali halides. It has therefore been suggested here that the observed EDC structure is more likely attributable to plasmon deexcitation. We conclude that more information is needed than is presently available in order to establish clearly the relative roles of these sources of EDC structure.

The shapes of the EDC's have been found to be essentially independent of the photon energy in the 0.1–10-keV region for metals (in an earlier work[1]) and for the semiconductors and insulators studied in the present work. This fact strongly supports the basic model assumption expressed in Eq. (1) that the principal secondary-electron excitation processes have effectively the same dependence upon the primary-electron energy and thus upon the energy of the incident photons.

Finally, with this model for x-ray photoemission, the dependence of the differential photocathode electron optical brightness β and of the total secondary-electron yield Y upon the photon excitation energy E_0 and upon the solid-state parameters of the emitter material E_G and E_A have been defined. It is hoped that this simple phenomenological model can help to guide the continuing research on the characterization of x-ray photoemission.

ACKNOWLEDGMENTS

This work is supported by a grant from the Air Force Office of Scientific Research, Grant No. 75-2762, and by a supplemental contract with the Department of Energy, Contract No. E(04-3)-235,

PA-15. The authors gratefully acknowledge the invaluable assistance, in the preparation of this report, of G. Gerhab, R. Hockaday, P. Piano, K. Premaratne, M. Schattenburg, M. Tester, and B. Young. We would also like to acknowledge the helpful suggestions of Professor William Pong of the University of Hawaii and of Professor Ryuichi Shimizu of the University of Osaka.

---

*Permanent address: La Trobe Univ., Dept. of Physics, Bundoora, Victoria, Australia 3083.
[1]B. L. Henke, J. A. Smith, and D. T. Attwood, J. Appl. Phys. 48, 1852 (1977).
[2]E. O. Kane, Phys. Rev. 147, 335 (1966).
[3]S. W. Duckett, Phys. Rev. 166, 302 (1968).
[4]D. C. Langreth, Phys. Rev. B 3, 3120 (1971).
[5]R. Stuart, F. Wooten, and W. E. Spicer, Phys. Rev. 135, A495 (1964).
[6]J. M. Ballantyne, Phys. Rev. B 6, 1436 (1972).
[7]G. A. Baraff, Phys. Rev. A 135, 528 (1964).
[8]M. S. Chung and T. E. Everhart, J. Appl. Phys. 45, 707 (1974).
[9]D. J. Bartelink, J. L. Moll, and N. I. Meyer, Phys. Rev. 130, 972 (1963).
[10]H. W. Streitwolf, Ann. Phys. 3, 183 (1959).
[11]O. Hachenberg and W. Brauer, *Advances in Electronics and Electron Physics* (Academic, New York, 1959), Vol. 11, p. 413.
[12]*Handbook of Mathematical Functions*, edited by M. Abramowitz and I. A. Stegun (Natl. Bur. Stand., Washington, D. C., 1964), Vol. 55, pp. 228-231.
[13]C. N. Berglund and W. E. Spicer, Phys. Rev. A 136, 1030 (1964).
[14]N. Schwentner, Phys. Rev. B 14, 5490 (1976).
[15]W. Kisiel and T. Lewowski, Acta Phys. Pol. A 45, 749 (1974).
[16]E. L. Garwin and J. Llacer, J. Appl. Phys. 41, 1489 (1970).
[17]F. Wooten, *Optical Properties of Solids* (Academic, New York, 1972), p. 159.
[18]C. Herring, Bell Syst. Tech. J. 34, 237 (1955).
[19]E. M. Conwell, Phys. Rev. A 135, 1138 (1964).
[20]C. R. Crowell and S. M. Sze, *Physics of Thin Films* (Academic, New York, 1967), Vol. 4, p. 325.
[21]B. L. Henke and E. S. Ebisu, *Advances in X-Ray Analysis* (Plenum, New York, 1974), Vol. 17, p. 150; B. L. Henke, *Advances in X-Ray Analysis* (Plenum, New York, 1976), Vol. 19.
[22]Similar measurements upon gold have been made, for example, by J. L. Gaines and R. A. Hansen, J. Appl. Phys. 47, 3923 (1976), and L. G. Eliseenko, V. N. Shchemelev, and M. A. Rumsh, Sov. Phys.—Tech. Phys. 13, 122 (1968).
[23]R. T. Poole, J. Liesegang, R. C. G. Leckey, and J. G. Jenkin, Phys. Rev. B 11, 5190 (1975); Phys. Rev. B 11, 5179 (1975).
[24]T. Miyakawa, J. Phys. Soc. Jpn. 24, 768 (1968).
[25]A. B. Kunz, T. Miyakawa, and S. Oyama, Phys. Status Solidi 34, 581 (1969).
[26]W. P. Menzel, K. Mednick, C. C. Lin, and C. F. Dorman, J. Chem. Phys. 63, 4708 (1975).
[27]L. J. Page and E. H. Hugh, Phys. Rev. B 1, 3472 (1970).
[28]W. Pong and C. S. Inouye, J. Electron Spectrosc. 11, 165 (1977).
[29]J. A. Knapp, G. J. Lapeyre, and P. L. Gobby, Bull. Am. Phys. Soc. 20, 474 (1975).
[30]N. O. Lipari and A. B. Kunz, Phys. Rev. B 3, 491 (1971).
[31]F. L. Battye, J. Liesegang, R. C. G. Leckey, and J. G. Jenkin, Phys. Rev. B 13, 2646 (1976).
[32]M. Creuzberg, Z. Phys. 196, 433 (1966).
[33]W. Pong and J. A. Smith, Phys. Rev. B 9, 2674 (1974).
[34]N. O. Lipari and A. B. Kunz, Phys. Rev. B 4, 4639 (1971).
[35]G. J. Lapeyre, J. Anderson, P. L. Gobby, and J. A. Knapp, Phys. Rev. Lett. 33, 1290 (1974).
[36]W. Pong and J. A. Smith, Phys. Rev. B 9, 2674 (1974).
[37]H. Overhof, Phys. Status Solidi B 43, 575 (1971).
[38]W. Pong and C. S. Inouye, Proceedings of the Fifth International Conference on Vacuum Ultraviolet Radiation Physics, Montpellier, France, September 1977 (unpublished).
[39]A. B. Kunz, Phys. Status Solidi 19, 115 (1968).
[40]C. S. Inouye and W. Pong, Phys. Rev. B 15, 2265 (1977). (1977).
[41]Y. Onodera, M. Okazaki, and T. Inui, J. Phys. Soc. Jpn. 21, 816 (1966); 2229 (1966).
[42]A. B. Kunz, J. Phys. Chem. Solids 31, 265 (1970).
[43]A. B. Kunz, Phys. Rev. 180, 934 (1969).
[44]Y. Onodera, J. Phys. Soc. Jpn. 25, 469 (1968).
[45]J. A. Smith and W. Pong, Phys. Rev. B 12, 5931 (1975).
[46]P. F. Best, Proc. Phys. Soc. 79, 133 (1962).
[47]M. Creuzberg and H. Raether, Solid State Commun. 2, 345 (1964).
[48]M. Creuzberg and H. Raether, Solid State Commun. 2, 175 (1964).
[49]C. J. Powell, Surf. Sci. 44, 29 (1974).